Wave Inversion Technology, Report No. 2, pages 115-132

Reservoir-scale In-situ Permeability Tensor from Induced Microseismicity

Serge A. Shapiro, Pascal Audigane, and Jean-Jacques Royer[1]

keywords: *permeability, hydrofracturing, fluid dynamics, poroelasticity*

ABSTRACT

We propose an approach for estimating the permeability tensor using seismic emission induced by borehole hydraulic tests or by a fluid injection of an arbitrary nature. This approach provides a single estimation of the permeability tensor for the complete heterogeneous rock volume, where the seismic emission was recorded. The approach is an extension of the method proposed by Shapiro et al, (1997) for isotropic case. It is based on the hypothesis, that the triggering front of the hydraulic-induced microseismicity propagates like the low-frequency second-type compressional Biot wave (corresponding to the process of the pore-pressure relaxation) in an effective homogeneous anisotropic poroelastic fluid-saturated medium. The permeability tensor of this effective medium is the permeability tensor of the heterogeneous rock volume upscaled to the characteristic size of the seismic-active region. We demonstrate the method using the microseismic data collected during the Hot-Dry-Rock Soultz-sous-Forêts experiment (Dyer et al., 1994). These data show that the corresponding rock volume is characterized by a significant permeability anisotropy caused by oriented crack systems. The maximal principal component of the permeability tensor has a subvertical orientation. It is about seven times larger than the minimal subhorizontal principal component.

INTRODUCTION

Fluid-injection tests in boreholes as well as perturbations of the pore pressure of a natural origin (e.g., rainfalls, water-level fluctuations in artificial lakes etc.) can generate a spontaneous seismic emission in rocks. In some locations the crust is in a failure equilibrium so that small perturbations of the pore pressure can modify the effective normal stress as well as the friction coefficients of the rock mass. This can lead to microearthquakes triggering.

[1]**email:** shapiro@ensg.u-nancy.fr

Recently, Shapiro et al. (1997) proposed to interpret the spatio-temporal evolution of the clouds of such microseismic events in terms of propagation of the so-called slow (second-type) Biot wave. In their approach, the real configuration of the fluid injection is assumed to be a point source of the pore pressure in an infinite homogeneous isotropic poroelastic saturated medium. In the low-frequency limit of the Biot equations (Biot 1962) the pore-pressure perturbation p can be approximately described by the following differential equation of diffusion:

$$\frac{\partial p}{\partial t} = D\nabla^2 p, \tag{1}$$

where D is the hydraulic diffusivity, and t is the time. This equation corresponds to the second-types Biot waves (the slow P-waves) in the low frequency limit and describes linear relaxation of pore-pressure perturbations.

It is important to note, that linear equation (1) was implicitly or explicitly used in many other works on the hydraulically induced seismicity (see, e.g., Nur and Booker, 1972, Ferreira et al, 1995, Fletcher and Sykes, 1977, Ohtake, 1974, and Talwani and Acree 1985).

In some situations (e.g., some hydrofracturing experiments) the hydraulic diffusivity can be changed considerably by the fluid injection. This means, that in equation (1) the quantity D must become pore-pressure dependent. Therefore, this equation becomes non-linear. Such changes of the diffusivity take place in restricted regions around boreholes. For instance, Cornet et al, 1997, proposed that in the Soultz borehole GPK1, which we discuss below, the opening of fractures due to the 'aseismic slip' can occur on distances of the order of 0.15km from the borehole. Due to such 'near-zone' effects also significant fluctuations of the fluid-flow rate can be observed (e.g, see Figure 2 from Cornet et al, 1997). However, our method is aimed to estimate the effective permeability in a large rock volume of the spatial scale of the complete reservoir. For example, in the case of Soultz, which we will refer to below this rock volume has the spatial characteristic size of the order of 1km.

Moreover, in a given elementary volume of the medium, the triggering of the earliest microseismic events starts already before the substantial relaxation of the pore-pressure occurs. This means, that even in the 'near zone' very earlier events occur in the practically unchanged medium. In other words, the front of significant changes of the medium propagates behind the quicker triggering front of earlier microseismic events. However, it is precisely these events that are important for our approach to estimating the permeability. Thus, the corresponding estimate should be approximately equal to the permeability of the unchanged medium even in such situations, where the permeability was strongly enhanced by the hydraulic fracturing.

Because of this reason we assume that changes of the diffusivity can be neglected. Thus, in eq. (1) D is assumed to be pressure independent.

Moreover, D is assumed to be homogeneously distributed in the medium. When estimating the diffusivity in such a way we replace the complete heterogeneous seismic-active rock volume by an effective homogeneous anisotropic poroelastic fluid saturated medium. The permeability tensor of this effective medium is the permeability tensor of the heterogeneous rock upscaled to the characteristic size of the seismic-active region. One can also call this effective-medium permeability tensor a 'global' permeability tensor or an 'apparent' permeability tensor. However, its physical meaning is well defined: it is the permeability tensor, which ensure that under an arbitrary pressure gradient in a homogeneous medium the vectors of the fluid-flow rate will coincide with the corresponding spatially averaged vectors of the flow rate caused by the same pressure gradient applied now to the actual heterogeneous seismic-active rock volume.

Let us now consider a step-function-like perturbation of the pore pressure at the injection source. For instance, this can be a rough approximation for the cases of a borehole-hydraulic fracturing (see, e.g., Figure 2 from Cornet et al, 1997) or rainfall-induced microseismicity. Shapiro et al. (1997) assumed that in a given elementary volume of the medium located at the distance r from the injection source, the triggering of microseismic events starts just before the substantial relaxation of the pore pressure has been reached. Taking into account that the high-frequency components of the pore-pressure perturbation (these components are characterized by a low energy) propagate quicker than the low-frequency components (these components are characterized by a high energy) they derived the following equation for the triggering front in an effective isotropic homogeneous poroelastic medium:

$$r = \sqrt{4\pi D t}. \tag{2}$$

This equation describes a spatial sphere, in the interior of which a substantial relaxation of the pore-pressure perturbation occurred to a given time t. Thus, with a correctly selected value of the hydraulic diffusivity, equation (2) corresponds to the upper bound of the cloud of events in the plot of their spatio-temporal distribution (i.e., the plot of r versus t).

Shapiro et al, (1997) used this approach for estimating the isotropic-effective-medium hydraulic diffusivity at KTB site. In Figure 1 such a spatio-temporal distribution of the microseismicity is shown for the the microseismic data collected during the Hot-Dry-Rock Soultz-sous-Forêts experiment in 1993 (see Dyer et al., 1994). In this figure the distances of hypocenters of about 9000 events from the source of the borehole-fluid injection (which was assumed to be located approximately at the depth 2920m of the borehole GPK1; for justification of this assumption see Section 5) are plotted as function of their occurrence times (see the more detailed description of the data below). In addition, two curves corresponding to equation (2) with $D = 0.05m^2/s$ and $D = 0.5m^2/s$ have been shown. It is clear that the curve with $D = 0.05m^2/s$ is in excellent agreement with the absolute majority of microseismic events. Such a remarkable agreement support the above concept of the triggering microseismicity.

However, the corresponding estimate of D is still a scalar.

In this paper, an extension of the method is developed in a way to consider the seismic-active rock volume as an effective homogeneous fluid-saturated poroelastic medium with an anisotropic permeability.

ANISOTROPIC PRESSURE RELAXATION

Assuming a homogeneous anisotropic medium, the equation of diffusion can be written in the principal axis:

$$\frac{\partial p}{\partial t} = \sum_{i=1}^{3} D_{ii} \frac{\partial^2 p}{\partial {x_i}^2}, \tag{3}$$

where D_{ii} are the principal components of the diffusivity tensor, and x_i are the spatial coordinates of points in the corresponding cartesian system.

Let us consider the following new system of coordinates, X_i:

$$X_i = \frac{x_i}{\sqrt{\varepsilon_i}}, \tag{4}$$

where $\varepsilon_i = 3D_{ii}/tr(\boldsymbol{D})$, $tr(\boldsymbol{D})$=$D_{11} + D_{22} + D_{33}$ and $\boldsymbol{D}$ is the hydraulic-diffusivity tensor. In this system, equation (3) becomes:

$$\frac{\partial p}{\partial t} = \frac{tr(\boldsymbol{D})}{3} \sum_{i=1}^{3} \frac{\partial^2 p}{\partial {X_i}^2}. \tag{5}$$

This equation is now equivalent to equation (1), i.e., it describes the isotropic relaxation of the pore pressure with the isotropic hydraulic diffusivity $\frac{tr(\boldsymbol{D})}{3}$. Thus, in the new coordinate system X_i, equation (2) keeps its form:

$$\sqrt{\sum_{i=1}^{3} {X_i}^2} = \sqrt{4\pi \frac{tr(\boldsymbol{D})}{3} t}, \tag{6}$$

where the left hand part of this equation is the radius in the new coordinate system. Taking the square of the radius and returning back to the principal coordinate system we obtain:

$$\sum_{i=1}^{3} \frac{{x_i}^2}{D_{ii}} = 4\pi t. \tag{7}$$

However, it is easy to see that in the principal coordinate system the following relationship is valid:

$$\sum_{i=1}^{3} \frac{{x_i}^2}{D_{ii}} = r^2 \boldsymbol{n}^T \boldsymbol{D^{-1}} \boldsymbol{n}, \tag{8}$$

where $r^2 = x_1^2 + x_2^2 + x_3^2$ is the radius in the principal coordinate system; $\boldsymbol{n} = \boldsymbol{r}/|\boldsymbol{r}|$, $\boldsymbol{r} = (x_1, x_2, x_3)^T$, T denotes that the matrix (vector) is transposed, and $\boldsymbol{D^{-1}}$ is the inverse matrix of $\boldsymbol{D}$. Therefore, the triggering front is now represented as follows:

$$r = \sqrt{\frac{4\pi t}{\boldsymbol{n}^T \boldsymbol{D^{-1}} \boldsymbol{n}}}. \tag{9}$$

Note that this equation holds its form in an arbitrary rotated (i.e., not necessary principal) coordinate system. Written in a simpler, characteristic for the principal coordinate system, form (see equation (7)) it shows that the triggering front is an ellipsoidal surface. Neglecting the elastic anisotropy in comparison with the flow anisotropy one can show that this surface has the same form as the group-velocity surface of the anisotropic slow (second-type Biot) wave.

NUMERICAL IMPLEMENTATION

To estimate the diffusivity tensor the entire space is divided in M directional sectors (in our case $M = 32$) centered at the injection point (see Figure 2). Each sector is defined by its maximal and minimal dips and its maximal and minimal azimuths. We define the azimuth and the dip to be comprised between $0°$ and $360°$ and between $-90°$ and $90°$, respectively. The dip is positive in the half space above the injection source. In each spatial sector the hydraulic diffusivity is estimated using the isotropic approach of Shapiro et al, (1997), i.e., using equation (2). Thus, M values of the hydraulic diffusivity are estimated for M different sectors of the space. We call them *directional diffusivities* D_i. The directional diffusivity D_i approximately characterizes the process of the pore-pressure relaxation along the direction $\boldsymbol{n_i}$ given by the dip and the azimuth of the central ray of i-th sector. On the other hand, the triggering front in an anisotropic medium is described by equation (9). Thus, the following system of matrix equations can be obtained from equations (2) and (9):

$$\boldsymbol{n_i}^T \boldsymbol{D^{-1}} \boldsymbol{n_i} = 1/D_i, \quad for \quad (i = 1, ..., M). \tag{10}$$

Taking into account the symmetry of the matrix $\boldsymbol{D}$, system (10) can be further transformed to the following large matrix equation:

$$\boldsymbol{A}\boldsymbol{X} = \boldsymbol{B}, \tag{11}$$

where $\boldsymbol{X} = (D_{11}^-, D_{22}^-, D_{33}^-, D_{12}^-, D_{13}^-, D_{23}^-)^T$; $\boldsymbol{B} = (1/D_1, ..., 1/D_M)^T$; D_{ij}^- are the terms of the inverse matrix $\boldsymbol{D^{-1}}$ and $\boldsymbol{A}$ is a rectangular $6 \times M$-matrix, whose i-th row is

$$n_{1i}^2,\ n_{2i}^2,\ n_{3i}^2,\ 2n_{1i}n_{2i},\ 2n_{1i}n_{3i},\ 2n_{2i}n_{3i}, \tag{12}$$

where n_{ji} is the j^{th} coordinate of the vector $\boldsymbol{n_i}$

Equation (11) provides each term of the hydraulic diffusivity tensor. For instance, the least-square method can be applied:

$$\boldsymbol{X^*} = (\boldsymbol{A^T A})^{-1} \boldsymbol{A^T B}, \tag{13}$$

where $\boldsymbol{X^*}$ is the least-square estimate of the vector $\boldsymbol{X}$. The 6×6 covariance matrix for the estimated components of matrix $\boldsymbol{D^{-1}}$ can be found as follows:

$$\boldsymbol{\sigma^2_{D^-}} = \sigma^2_R (\boldsymbol{A^T A})^{-1}, \tag{14}$$

where

$$\sigma^2_R = \frac{||\boldsymbol{B} - \boldsymbol{A X^*}||^2}{M - 6}. \tag{15}$$

In order to estimate the diffusivity tensor the estimated matrix $\boldsymbol{D^{-1}}$ should be inverted and diagonalized. In order to estimate the uncertainties of the diffusivity tensor we should twice repeat this procedure, but now the components of matrix $\boldsymbol{D^{-1}}$ should be reduced and increased to the amount of square roots of corresponding diagonal components of matrix $\boldsymbol{\sigma^2_{D^-}}$. In the following section we show results of this computations for the Soultz example.

CASE STUDY: SOULTZ-SOUS-FORETS

Before to proceed further with a particular example we would like to emphasize that the approach elaborated above is rather general and can be applied to many situations, where a fluid injection of an artificial or a natural origin induces the seismic emission.

Let us now illustrate the approach by applying it to one of the hydrofracturing experiments performed by SOCOMINE (France) and CSMA (UK) in Soultz-sous-Forêt (Alsace, France).

The Hot-Dry-Rock project in Soultz-sous-Forêt uses the geothermal anomaly of the Rhine Graben to produce geothermal energy (Gérard et al, 1994; Baria et al, 1995; Kappelmeyer et al, 1991). To elaborate this project, two wells, GPK1 and GPK2 were drilled to the depth of 3600 m and 3800 m, respectively. In order to stimulate the fracture network in the granite environment different phases of the hydraulic fracturing were performed. During these hydraulic tests, a seismic monitoring was carried out (Dyer et al, 1994; Beauce at al, 1995). A large-scale cloud of microevents has been observed.

Here, we consider the GPK1 fracturing experiment conducted from 1 to 22 September 1993. During this test $25000\ m^3$ of water was injected. More than 9300 microseismic events were localized during the injection phase (1 to 17 September; these events are shown in Figure 1). Microseismicity was activated by the injection pressure

of around 60 bars (6 MPa). The cloud of the microseismic events was extended from the casing shoe (2800-3000 m) to the depth of 3400 m. The major orientation tendencies of the cloud are close to the stress tensor orientation, that is, subvertical NW/SE, in the upper part, and subvertical N/S at the bottom (see Dyer et al, 1993; further references and data on stress can be found in Klee & Rummel, 1993 and Cornet et al, 1997). First hydraulic-based calculations provided an estimate of the permeability of the order $10^{17} - 10^{-16} m^2$ (see e.g., Jung et al, 1996 and Jung et al, 1995).

If we consider the process of the pore-pressure relaxation in this experiment as isotropic one, Figure 1 will provide the following estimate of the permeability: $5 \times 10^{-17} m^2$ (see below for explanations how to estimate the permeability from the hydraulic diffusivity). However, it is easy to see that this process is not isotropic. Indeed, Figures 3 nad 4 show the cloud of the microearthquakes in the top- and North view for the time intervals of 100, 200, 300 and 400 hours after the start of the injection. Taking into account the scales of these Figures (approximately, the vertical and horizontal sizes of the boxes in the top view are 1130m and 620m, respectively; these of the North view are 1430m and 800m, respectively) we can see that the growth velocities of the cloud are different in different directions. Moreover, very roughly we can describe the process by a growing ellipsoid.

Further, by extrapolation to the time 0 this representation allows to roughly localize the injection point on the well at the depth approximately equal to 2920 m. This depth approximately corresponds to the center of the depth interval $2850 - 3000m$, where flow logs show a major part of the fluid loss (60%, see for detailed references Cornet et al, 1997) from the borehole to the surrounding rocks. Thus, we approximate the real configuration of the injection test by the point injection at the depth of 2920 m. This point was used to compute the distances from the injection source to the seismic events (see Figures 1, 5 and 6).

After subdivision of the space into $M = 32$ sectors we applied the inversion described in the previous section. For example, Figures 5 and **??** show spatio-temporal distribution of microseismic events included in two different spatial sectors. For the sector 1, the azimuth is comprised between $315°$ and $270°$ and the dip between $-90°$ and $-45°$. In the sector 2, the azimuth is comprised between $225°$ and $180°$ and the dip between $-90°$ and $-45°$. These two sets of points allow to estimate two directional diffusivities of the order of $0.01\, m^2 s^{-1}$ and $0.035\, m^2 s^{-1}$ respectively. This illustrates the anisotropy of the hydraulic diffusivity.

It is important to note here, that the only objective criterion to finding upper boundaries of point sets of the spatio-temporal distributions of events is that the parabolic curve should be an envelope for the absolute majority of the points. A formal criterion for this is a question of a mainly heuristic choice. For example in Soultz we looked for parabolic curves 98% of points were below of them. We return to this issue once more in the Discussion.

Having the directional diffusivities estimated as described above equations (13)-(15) provide the following principal components of the hydraulic-diffusivity tensor along with the estimates of their σ-order confident intervals:

$$\boldsymbol{D} = \begin{pmatrix} 0.6 \pm 0.2 & 0 & 0 \\ 0 & 1.7 \pm 0.3 & 0 \\ 0 & 0 & 4.6 \pm 2.4 \end{pmatrix} 10^{-2} m^2 s^{-1} \tag{16}$$

To compare the anisotropy of the permeability with the geometrical features of the cloud we computed the covariance matrix $\boldsymbol{C} = \{C_{ij}\}$ centered at the injection point:

$$C_{ij} = \frac{1}{n} \sum_{k=1}^{n} (x_i(k) - m_i)(x_j(k) - m_j), \tag{17}$$

where n is the total number of events, $x_i(k)$ are coordinates of the k-th event and m_i are the coordinates of the injection source. Note, that the matrix $\boldsymbol{C}$ is directly related to the inertia tensor. Its principal directions show the principal-rotation axes of the seismicity cloud.

The computations show that orientations of the principal components of the two tensors are slightly different. They have a similar subvertical maximum-value directions, with the dip close to $E75°$ for the matrix $\boldsymbol{C}$ and $W80°$ for the diffusivity tensor. The azimuth of the second-large (quasi horizontal) principal component for the diffusivity tensor is close to $N130°$. At the same time, the cloud of microevents is preferably oriented along $N170°$. However, the directional resolution of our computations (the angular size of each sector is about $40°$) does not permit to confidently distinguish between these two directions. We can state only that the both tensors show subvertical orientation of the maximal principal components and NW/SE to N/S orientation of the largest subhorizontal principal component.

The relationship between the tensor of the hydraulic diffusivity and the tensor of permeability can be derived from the Biot equations (Biot, 1962). The tensorial form of the corresponding equation of Shapiro et al., (1997) is as follows:

$$\boldsymbol{D} = N\boldsymbol{K}/\eta, \tag{18}$$

where $\boldsymbol{K}$ is the permeability tensor, η is the pore-fluid dynamic viscosity and N is a poroelastic modulus which for the case of low-porosity crystalline rocks can be approximated as follows:

$$N = \left[\frac{\phi}{K_f} + \frac{\alpha}{K_g} \right]^{-1}, \tag{19}$$

where $\alpha = 1 - K_d/K_g$, ϕ is the porosity , and K_d, K_g, K_f, are, respectively, bulk modules of the dry frame, of the grain material and of the fluid. Note, that we neglected here the elastic anisotropy in comparison with the anisotropy of the permeability.

According to the log measurements and literature data, we accepted the following estimates: $\phi = 0.003$, $\eta = 1.9\ 10^{-4}$ Pa.sec.(dynamic viscosity of a salt water at $150°$, Haar et al., 1984), $K_d = 49$ GPa, $K_g = 75$ GPa and $K_f = 2.2$ GPa. Thus $N \approx 1.68\ 10^{11}$ Pa and the permeability tensor is:

$$\boldsymbol{K} = \begin{pmatrix} 0.7 \pm 0.2 & 0 & 0 \\ 0 & 1.9 \pm 0.3 & 0 \\ 0 & 0 & 5.2 \pm 2.6 \end{pmatrix} 10^{-17} m^2 \qquad (20)$$

DISCUSSION

The first aspect we should discuss is the relationship between the orientation of the microseismicity cloud and the orientation of the permeability tensor. The permeability tensor characterizes the magnitude and the orientation of the growth rate of the seismicity cloud. Generally, the symmetry of the growth rate can differ from the symmetry of the cloud itself. Therefore, in principle, the inertia tensor of the microseismicity cloud can have a different orientation than the permeability tensor.

The approach described here requires a very large number of events for a reliable estimation of the orientation of the permeability tensor. In the particular case of Soultz considered here we cannot confidently distinguish between the orientations of the permeability and the inertia tensors. However, there may exist natural reasons for this. For instance, it is probable that in fractured reservoirs the symmetry of microseismicity clouds coincides with the symmetry of filtration-path distributions.

Studies on cores collected on the wells at Soultz have revealed a high density fracturing systems associated to $N0°$ and $N170°$ direction at the core-scale (Genter et al, 1997; Dezayes et al, 1995; Ledésert et al, 1993; Tenzer et al, 1991), and to $N130°$ and $N40°$ at the micro-scale (Schild et al., 1998). Hence, the obtained orientation of the permeability tensor, in principle, is in agreement with the observed fracturing orientation.

Let us discuss another facet of the method. The isotropic method of Shapiro et al. (1997) tends to provide the upper limit of the hydraulic-diffusivity estimates mainly due to the two reasons. The first one is that in the case of the hydraulic fracturing, we cannot completely exclude the injection caused permeability enhancement in the borehole adjacent domain. However, we think that this enhancement is of a very restricted significance because the estimates of the hydraulic diffusivity are based on parameters of the outer parabolic boundary of the spatio-temporal distribution of microevents. Thus, the permeability estimates are related to an early low-energetic triggering front propagating in the as yet practically unchanged medium (see also the Introduction). Indeed, the prior to hydrofracturing hydraulic-based determinations of the apparent permeability for the GPK1 depth interval $2850 - 3400m$ provided value of $2.5 \times 10^{-17} m^2$

(Jung et al, 1996). This is in a good agreement with the above results for the permeability tensor. Thus, the method indeed provides a pre-hydrofracturing permeability. This is also indirectly confirmed by new calculations (Shapiro et al, 1998) which we have performed for the microseismic activity induced by later injection tests (1995-1996) in GPK2. The corresponding (isotropic) estimates of the diffusivity prior to the stimulation were of the same order as shown here. After the stimulation they became five to ten times higher than those obtained here. Therefore, we were able to estimate these changes, i.e., the method allows to quantify and to monitor the hydrofracturing impact on rock masses.

The second (more general) reason, why the method tends to provide the upper bound of the permeability is hidden in the very nature of the approach. We are looking for the upper bound of the point multitude on the plot of the spatio-temporal distribution of events. Following this principle, our calculations also give the upper-bound for the permeability tensor. It is clear now, that the plot of the complete spatio-temporal distribution of microevents provides an estimate, which should be close to the largest principal component of the permeability tensor. This is also the case for the considered example of Soultz (see Figure 1).

Note also, that the criteria for fitting the upper parabolic boundaries to spatio-temporal distributions of events are of partially heuristic character. These curves should be envelopes for the absolute majority of events. In the case of Soultz we looked for envelopes of 98% of all points. In fact, very similar semi-heuristic character has the numerical coefficient under square root of equation (2). Considering the characteristic frequencies of pore-pressure perturbations Shapiro et al (1997) proposed that this coefficient should be approximately equal to 4π. However, this coefficient, as well as the fitting criteria can be improved by a calibration of the diffusivity estimates with available results of large-scale hydraulic tests. It is interesting to note, that the good agreement between the estimated here permeability tensor and the previous hydraulic-based estimates was obtained without any calibration. Thus, the criteria and coefficients used here are appropriate. Moreover, it is important to understand that the results the method provides on *the spatial orientation of the permeability tensor and its anisotropy (i.e., principal-component proportions) are completely objective and does not require any calibration*.

Before to conclude the discussion, we should once more point out the upscaling (i.e., effective-medium) character of the permeability-tensor estimates providing by the method (see Introduction). This means that all, the values of the principal components of the permeability, as well as their orientation and proportions (i.e., the permeability anisotropy), is influenced by smaller-scale local heterogeneities.

Finally, it is interesting to note that the characteristic, parabolic-bounded-domain behavior of the spatio-temporal distributions of the injection-induced seismic emission can be widely observed (see for example Figure 2 from Fehler et al, 1998). An appropriate interpretation of such data can provide hydraulic properties of rocks in-situ.

CONCLUSIONS

A new method for estimating the in-situ reservoir-scale permeability tensor using the microseismic emission induced during a fluid injection has been developed. According to the data provided by the Hot-Dry-Rock site of Soultz-sous-Forêts, the permeability tensor obtained is in a good agreement with the previous hydraulic estimations. Its orientations and principal components reveal a significant subvertical tendency for a maximal permeability of $(5.2 \pm 2.6)\, 10^{-17} m^2$. This corresponds to the fractured granite permeability of Soultz-sous-Forêts before hydrofracturing.

ACKNOWLEDGMENT

We are grateful to A. Beauce (BRGM), R. Jones (CSMA) and A. Gérard (SOCOMINE) for their help with accessing the basic data on the fluid-injection induced seismicity in the Soultz-sous-Forêts site.

REFERENCES

Baria, R., Garnish, J., Baumgartner, J., Gérard, A., and Jung, R., 1995, Recent developments in the European HDR research programme at Soultz-sous-Forêts (France): Proceedings of the World Geothermal Congress, 1995, Florence, Italy, 2631–2637.

Beauce, A., Fabriol, R. J. H., and Hulot, C., 1995, Seismic studies on the Soultz HDR project (France) during phase Iia.: Geotherm. Sci. Techn., **4**, 253–272.

Biot, M. A., 1962, Mechanics of deformation and acoustic propagation in porous media: Journal of Applied Physics, **33**, 1482–1498.

Cornet, F. H., Helm, J., Poitrenaud, H., and Etchecopar, A., 1997, Seismic and aseismic slips induced by large-scale fluid injections: Pure appl. geophys., **150**, 563–583.

Dezayes, C., Villemin, T., Genter, A., Traineau, H., and Angelier, J., 1995, Analysis of fractures in boreholes of the Hot Dry Rock project at Soultz-sous-Forêts (Rhine Graben, France: Sci. Drilling, **5**, 31–41.

Dyer, B., Juppe, A., Jones, R. H., Thomas, T., Willis-Richards, J., and Jaques, P., Microseismic Results from the European HDR Geothermal Project at Soultz-sous-Forets, Alsace, France:, CSM Associated Ltd, IR03/24, 1994.

Fehler, M., House, L., Phillips, W. S., and Potter, R., 1998, A method to allow temporal variation of velocity in travel-time tomography using microearthquakes induced during hydraulic fracturing: Tectonophysics, **289**, 189–202.

Ferreira, J. M., Oliveira, R. T. D., Assumpcao, M., Moreira, J. A. M., Pearce, R., and Takeya, M. K., 1995, Correlation of seismicity and water level in the acu reservoir - an example from northeast brazil: Bulletin of the Seismological Society of America, **85**, no. 5, 1483–1489.

Fletcher, J. B., and Sykes, L. R., 1977, Earthquakes Related to Hydraulic Mining and Natural Seismic Activity in Western New York State: Journal of Geophysical Research, **82**, 3767–3780.

Genter, A., Castaing, C., Dezayes, C., Tenzer, H., Traineau, H., and Villemin, T., 1997, Comparative analysis of direct (core) and indirect (borehole imaging tools) collection of fracture data in the Hot Dry Rock Soultz reservoir (France): Journal of Geophysical Research, **102**, no. B7, 15419–15431.

Gérard, A., Jung, R., and Moore, P. L., Situation of the European Hot dry Rock Project at Soultz-sous-Forets:, Internal CEE Report - Socomine-BGR-SII, 1994.

Haar, L., Gallagher, J., and Kell, G., 1984, NBS/NRC Steam Tables; Thermodynamic and transport properties and computer programs for vapor and liquid states of water in SI units: Hemispher Publishing Corporation, New York, 320p, New York, 1 edition.

Jung, R., Willis-Richard, J., Nicholls, J., Bertozzi, A., and Heinemann, B., 1995, Evaluation of hydraulic tests at Soultz-sous-Forêts, European HDR site: Proceedings of the World Geothermal Congress, 1995, Florence, Italy, 2671–2676.

Jung, R., Cornet, F., Rummel, F., and Willis-Richard, J., 1996, Hydraulic stimulation results 1992/1993: R. Baria, J. Baumgärtner and A. Gérard (editors): European Hot Dry Rock Programme, 1992 - 1995. Extended Summary of the Final Report to European Community (DG XII), Contract N JOU2-CT92-0115 (Date of issue: 28 March 1996, Version 1)., 31–41.

Kappelmeyer, O., Gérard, A., Schloemer, W., Ferrandes, R., Rummel, F., and Benderitter, Y., 1991, European HDR project at Soultz-sous-Forêts general presentation: Geotherm. Sci. Techn., **2**, 263–289.

Klee, G., and Rummel, F., 1993, Hydrofrac stress data for the european HDR research project test site Soultz-sous-Forêts: Int. J. Rock Mech. Min. Sci. & Geomech. Abstr., **30**, no. 7, 973–976.

Ledésert, B., Dubois, J., Genter, A., and Meunier, A., 1993, Fractal analysis of fracture applied to Soultz-sous-Forêts Hot Dry Rock geothermal program : J. Volcanol. Geotherm. Res., **57**, 1–17.

Nur, A., and Booker, J., 1972, Aftershocks caused by pore fluid flow?: Science, **175**, 885–887.

Ohtake, M., 1974, Seismic activity induced by water injection at Matsushiro, Japan: J. Phys. Earth, **22**, 163–176.

Schild, M., Vollbrecht, A., Siegesmund, S., and Reutel, C., 1998, Microcracks in granite cores from the EPS-1 geothermal drill hole, Soultz-sous-Forêts (France): paleostress directions, paleofluids and crack-related Vp-anisotropies: Geol Rundsch, **86**, 775–785.

Shapiro, S. A., Huenges, E., and Borm, G., 1997, Estimating the crust permeability from fluid-injection-induced seismic emission at the KTB site: Geophysical Journal International, **131**, F15–F18.

Shapiro, S. A., Royer, J.-J., and Audigane, P., 1998, Estimating the Permeability from Fluid-Injection Induced Seismic Emission: Thimus J.-F., Abousleiman Y., Cheng A.H.-D., Coussy O. and E. Detournay, Eds., Poromechanics, 301–305.

Talwani, P., and Acree, S., 1985, Pore pressure diffusion and the mechanism of reservoir-induced seismicity: Pure appl. geophys., **122**, 947–965.

Tenzer, H., Mastin, L., and Heinemann, H., 1991, Determination of planar discontinuities and borehole geometry in the crystalline rock of borehole GPK-1 at Soultz: Geotherm. Sci. Techn., **3**, 31–67.

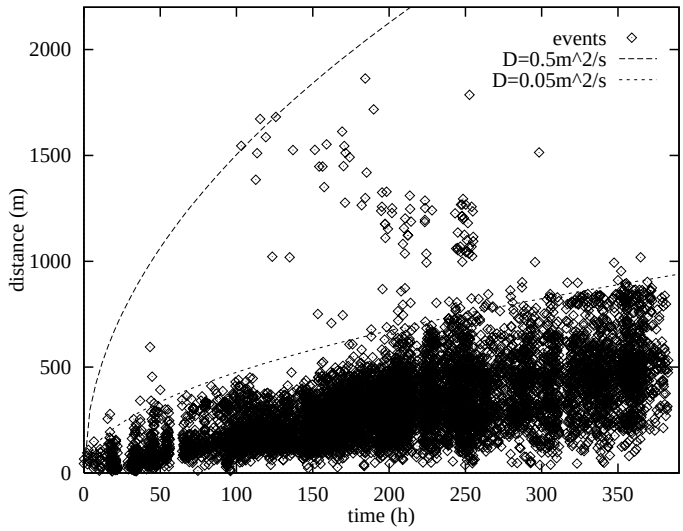

Figure 1: Distances of the events from the injection source versus their occurrence time for the Soultz-Sous-Forets experiment: Borehole GPK1, September 1-22, 1993. For this figure the complete cloud of the microseismicity recorded during the injection time (1-17 Sept.) was used.

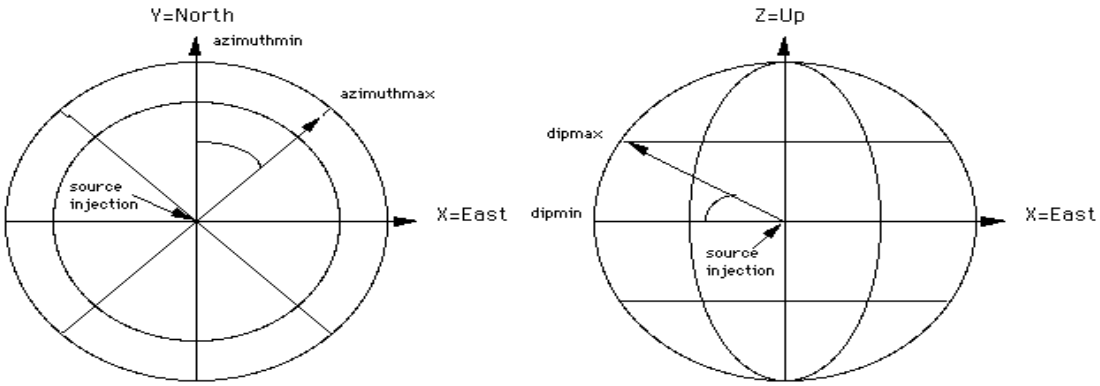

Figure 2: Scheme of the space decomposition in 32 sectors.

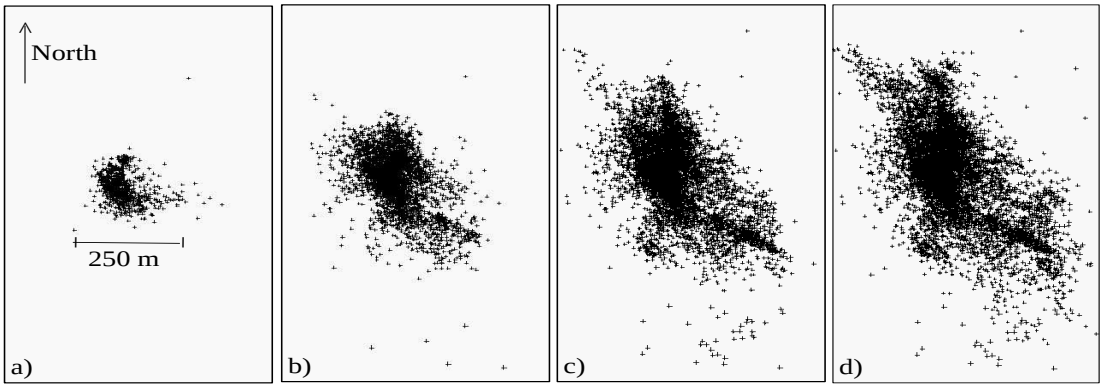

Figure 3: The top view of the microseismic cloud a)100 h, b)200 h, c)300 h, d)400 h after the start of the injection.

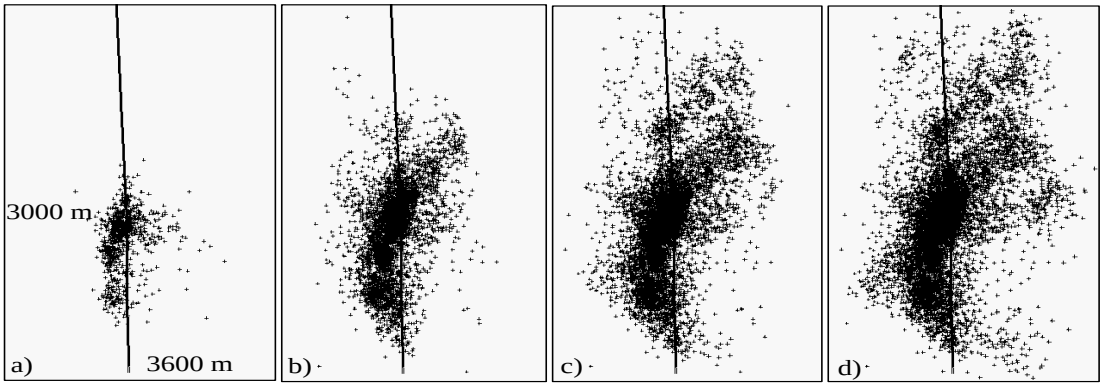

Figure 4: The the North view of the microseismic cloud a)100 h, b)200 h, c)300 h, d)400 h after the start of the injection.

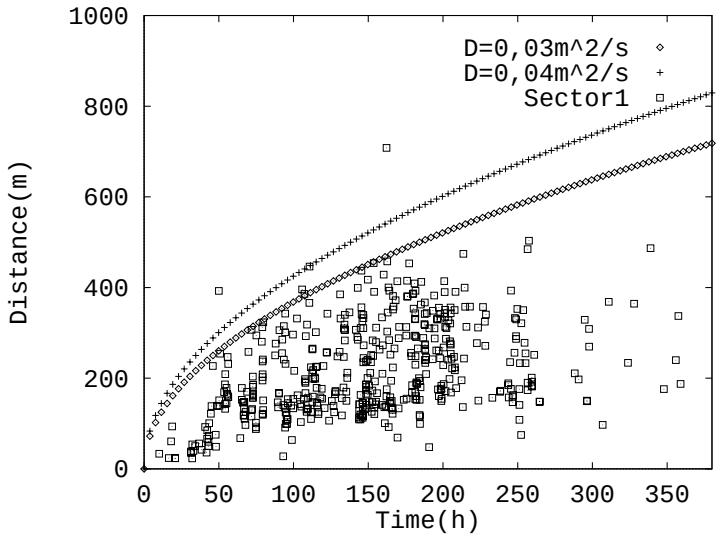

Figure 5: Distances of the events from the injection source versus their occurrence time in the spatial sector 1 (azimuth= $292.5° \pm 22.5°$, dip=$-67.5° \pm 22.5°$)

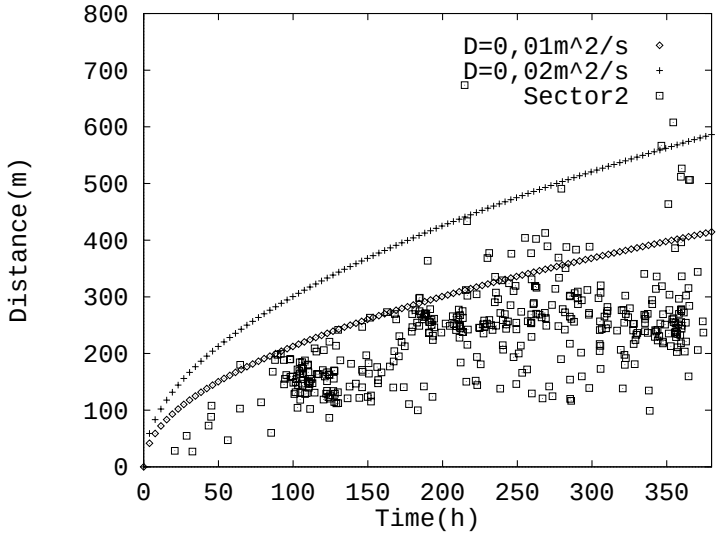

Figure 6: Distances of the events from the injection source versus their occurrence time in the spatial sector 2 (azimuth= $202.5° \pm 22.5°$, dip=$-67.5° \pm 22.5°$)